Investigating the temporal dynamics of continuously pumped Nd:YVO_4 self-Raman lasers: observation of self-mode-locking

2013 Laser Phys. 23 095804

(http://iopscience.iop.org/1555-6611/23/9/095804)

IOP PUBLISHING LASER PHYSICS
Laser Phys. **23** (2013) 095804 (5pp) doi:10.1088/1054-660X/23/9/095804

Investigating the temporal dynamics of continuously pumped Nd:YVO_4 self-Raman lasers: observation of self-mode-locking

Y C Lin, C Y Lee, W Z Zhuang, K W Su and Y F Chen[1]

Department of Electrophysics, National Chiao Tung University, Hsinchu 30010, Taiwan

E-mail: yfchen@cc.nctu.edu.tw

Received 7 June 2013
Accepted for publication 29 July 2013
Published 19 August 2013
Online at stacks.iop.org/LP/23/095804

Abstract
We experimentally investigate the temporal dynamics of continuously pumped Nd:YVO_4 self-Raman lasers. In the single-transverse-mode operation, it is found that the temporal behavior of the self-Raman laser exhibits a regular pulse train similar to the phenomenon of self-mode-locking. In the multi-transverse-mode operation, the average output power can be scaled up to 1.1 W and the temporal feature displays a complex dynamics that is numerically reconstructed with simultaneous longitudinal and transverse mode-locking.

(Some figures may appear in colour only in the online journal)

1. Introduction

In recent years, the search for optical crystals with high gain coefficients of the stimulated Raman scattering (SRS) has been a resurgent topic with the advent of the all-solid-state laser technologies [1–10]. Among promising crystals for efficient SRS, the self-Raman gain media that combine the laser emission and SRS wavelength conversion in single crystals have attracted particular interest because they can be employed to realize the so-called self-Raman lasers with compactness and high efficiency. So far, the widely used self-Raman active media include Yb:$KGd(WO_4)_2$ [1], Nd:$PbWO_4$ [2], Nd:$KGd(WO_4)_2$ [3], Nd:$Gd_xY_{1-x}VO_4$ [4], Nd:$GdVO_4$ [5], and Nd:YVO_4 [6, 7] crystals. The Q-switched approaches [1–6] were utilized in the earlier self-Raman lasers to enhance the SRS efficiency with high peak powers. Since the first realization of continuous-wave (CW) Nd:$KGd(WO_4)$ Raman lasers [11], there is much attention on developing CW self-Raman lasers due to their potential applications in optical communications and biomedicine [12–18].

In the past few years, self-Raman gain media such as Nd:YVO_4 and Nd:$GdVO_4$ crystals have been employed to realize the self-mode-locking without any saturable absorber in the CW pumping scheme [19–23]. Therefore, it is of great interest whether the CW self-Raman lasers also display a temporal behavior similar to the self-mode-locking. Even though Lisinetskii *et al* [24] have observed the self-mode-locked phenomenon at the second and fourth Stokes generations in a pulse-pumped solid-state laser, up to now there is no detailed exploration for the temporal dynamics of CW diode-pumped self-Raman lasers.

In this work, we exploit a double-end diffusion-bonded YVO_4/Nd:YVO_4/YVO_4 crystal to achieve the self-Raman operation for exploring the temporal dynamics. We firstly use a low-power laser diode to obtain a self-Raman laser at 1176 nm in the single-transverse-mode operation. With a pump power of 1.7 W, the average Raman output is found to be 80 mW. Under this circumstance, the temporal trace displays a continuous pulse train with pulse duration of 10.6 ps, and the pulse period is equal to the cavity

[1] Address for correspondence: Department of Electrophysics, National Chiao Tung University, 1001 TA Hsueh Road, Hsinchu 30050, Taiwan.

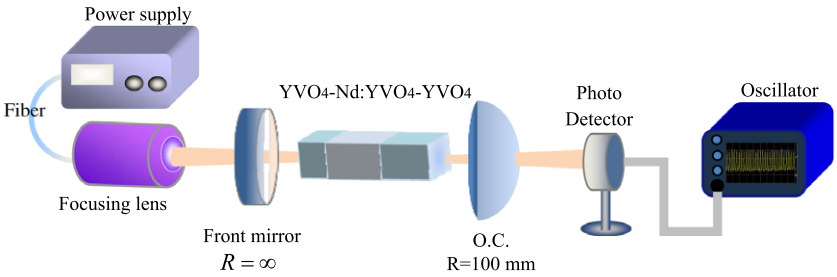

Figure 1. Experimental setup for a CW diode-pumped Nd:YVO_4 self-Raman laser with a plano-concave resonator.

round-trip time. For scaling up the output power, we employ a high-power laser diode to obtain a self-Raman laser in the multi-transverse-mode operation. With a pump power of 15.5 W, we attain a self-Raman laser with the output power up to 1.1 W. In the multi-transverse-mode operation, we experimentally observe that the Raman output exhibits the characteristics of complex spatiotemporal dynamics. We numerically analyze the experimental data to confirm that the spatiotemporal features originate from the mode-locking of fundamental and high-order transverse modes.

2. Experimental setup

Figure 1 depicts the experimental setup for a CW diode-pumped Nd:YVO_4 self-Raman laser with a plano-concave resonator. The cavity mirrors were coated for the intracavity SRS wavelength conversion from the fundamental wavelength of 1064 nm to the first Stokes output of 1176 nm. The input flat mirror has antireflection coating at 808 nm ($R < 0.2\%$) on the entrance face, high-reflection (HR) coating at 1000–1200 nm ($R > 99.8\%$), and high-transmission (HT) coating at 808 nm ($T > 95\%$) on the other surface. The output coupler (OC) is a 100 mm radius-of-curvature concave mirror with HR coating at 1064 nm ($R > 99.8\%$) and 1176 nm ($R > 99\%$). The active medium is an *a*-cut 4 mm × 4 mm × 20 mm double-end diffusion-bonded 0.3-at.% Nd^{3+}-doped Nd:YVO_4 crystal bonded with a 2 mm long and an 8 mm long undoped YVO_4 end at its pumped facet and the other facet, respectively. The diffusion-bonded crystal can effectively reduce the thermal effects and increase the interaction length for the SRS [25]. Both sides of the active medium were coated for antireflection at 1000–1200 nm ($R < 0.2\%$). Additionally, the active medium was wrapped with indium foil and mounted in a water-cooled cooper block with water temperature to be maintained at 12 °C. Since the intracavity SRS efficiency is significantly sensitive to the cavity losses and thermal effects, the cavity length has to be as short as possible. Consequently, the separation of the cavity mirrors was approximately 26 mm, corresponding to an optical path length of ∼50 mm.

The temporal dynamics of the laser output were detected by a high-speed InGaAs photodetector (Electro-optics Technology ET-3500) with rise time 35 ps. The output signal of the photodetector was connected to a digital oscilloscope (Agilent, DSO 80000) with 12 GHz electrical bandwidth and sampling interval of 25 ps for real-time monitoring. In the meanwhile, the output signal was employed to measure the power spectrum with an RF spectrum analyzer (Advantest, R3265A) with 8-GHz bandwidth. It is worth noting that, since the longitudinal mode spacing of the cavity is up to 3 GHz, the electrical bandwidths of the detector and instrument have to be high enough for real-time observation. The optical spectrum of the laser output was measured with a Fourier–Michelson optical interferometer (Advantest, Q8347) with a resolution of 0.003 nm.

3. Experimental results and discussion

To begin with, we utilized a 2-W fiber-coupled 808-nm laser diode with a core diameter of 100 μm to obtain a single-transverse-mode self-Raman output. Using a lens of 25-mm focal length and 85% coupling efficiency, the pump source was focused into the laser crystal with an average pump radius of 60 μm. With the cavity mode size of 128 μm, the pump-to-mode-size ratio was approximately 0.47. Figure 2(a) shows the average output powers at the fundamental wavelength of 1064 nm and the first Stokes wavelength of 1176 nm with respect to the incident pump powers. The threshold for self-Raman output was near 0.52 W. With a pump power of 1.7 W, the average output power at the first Stokes wavelength was measured to be approximately 80 mW. For the pump power in the range of 0.52 and 1.14 W, the optical spectrum revealed the self-Raman laser to be in the single-longitudinal-mode operation. While the incident pump power increased above 1.14 W, the self-Raman output could be found to step into the multi-longitudinal-mode operation with an apparent self-mode-locked phenomenon in the real-time traces. Figures 2(b)–(d) show the measured results for the self-mode-locking of the self-Raman laser at the pump power of 1.7 W. As seen in figure 2(b), the main peak in the power spectrum exactly corresponds to the longitudinal mode spacing of 2.93 GHz. The temporal trace shown in figure 2(c) demonstrates the pulse train to be in the mode-locked state without significant CW background. The full width at half maximum (FWHM) of the autocorrelation trace was measured to be approximately 15 ps, as displayed in figure 2(d). The mode-locked pulse duration was thus estimated to be 10.6 ps, assuming the temporal intensity is a Gaussian profile.

Next, we used a 20-W fiber-coupled 808-nm laser diode with a core diameter of 400 μm to scale up the self-Raman output power. Under the same cavity configuration, the pump radius was approximately 240 μm and the pump-to-mode

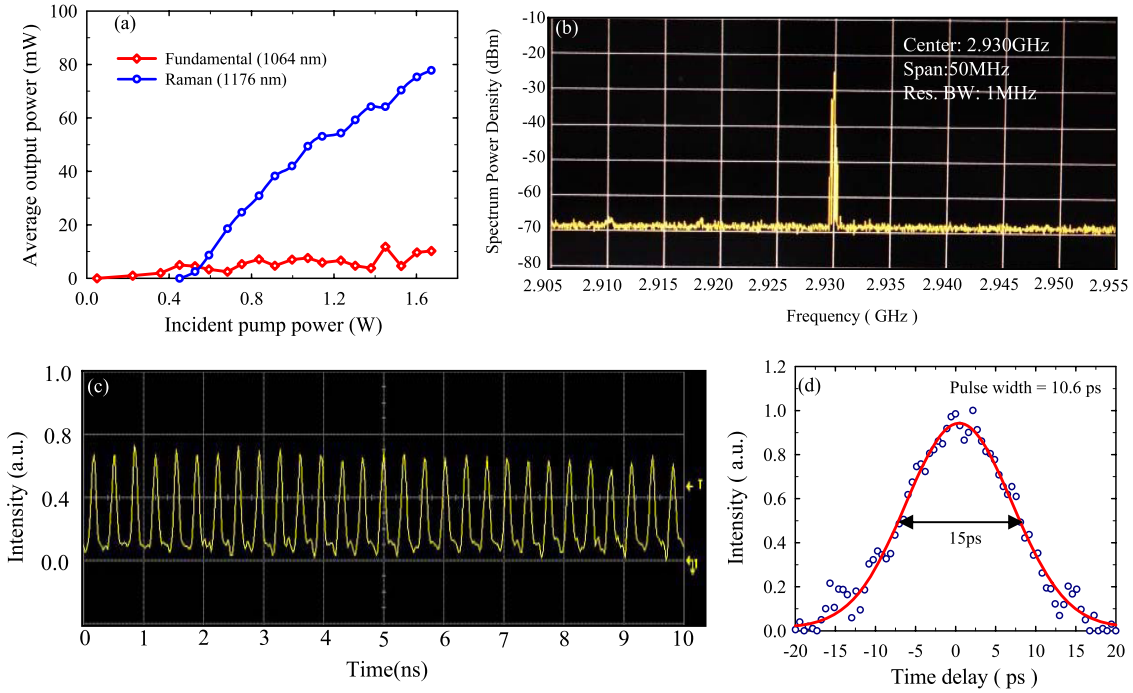

Figure 2. (a) The average output power at the fundamental wavelength of 1064 nm and the first Stokes wavelength of 1176 nm with respect to the incident power; (b) experimental results of the power spectrum at incident pump power of 1.7 W; (c) pulse train for the mode-locking of single transverse TEM_{00} modes; (d) corresponding autocorrelation trace of the output pulses.

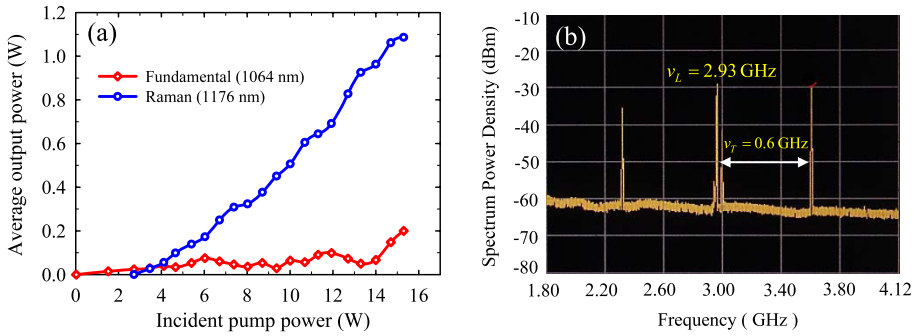

Figure 3. (a) The average output power at 1064 and 1176 nm versus the incident pump power for a higher-power diode-pumped source; (b) power spectrum at an incident pump power of 15.5 W.

size ratio could be found to be in the region of 1.9. As a result, in addition to the fundamental TEM_{00} modes, some high-order transverse modes might be simultaneously excited [26]. Figure 3(a) shows the average output powers versus the incident pump powers for the fundamental and the first Stokes wavelength. The threshold for self-Raman output was approximately 2.72 W. With a pump power of 15.5 W, the average output power at the first Stokes wavelength was found to be up to 1.1 W. Experimental optical spectra revealed that for pump power greater than 3.5 W the self-Raman laser started being in self-mode-locked operation. Figure 3(b) shows the experimental measurement for the power spectrum of Raman output at the pump power of 15.5 W. It can be seen that there are two peaks with frequency difference in the range of 0.6 GHz to the main peak at 2.93 GHz. The beating frequency of 0.6 GHz is consistent with the transverse mode spacing of the cavity. We used a CCD camera to measure the beam profile of self-Raman output, as depicted in figure 4(a). The individual temporal traces for the three positions labeled 1–3 in figure 4(a) are shown in figures 4(b)–(d). The coordinates for labels 1–3 with the unit of mm are $(x, y, z) = (0.05, 0.05, 400)$, $(x, y, z) = (0.4, 0.1, 400)$, and $(x, y, z) = (0.85, 0, 400)$, respectively. The time traces can be seen to display a phenomenon of spatiotemporal dynamics. In the following, we reconstructed the experimental data to demonstrate that the spatiotemporal characteristics are caused by the total self-mode-locking of fundamental and higher-order transverse modes [27–29].

The wavefunction of a free-space Hermite–Gaussian mode in terms of the Cartesian coordinates (x, y, z) and time t under the paraxial approximation can be written as [26]

$$\Phi_{n,m,l}(x, y, z, t) = \psi^{(\mathrm{HG})}_{n,m}(x, y, z, t)\, \mathrm{e}^{-\mathrm{i}\, l\, \Omega_{\mathrm{L}}\, t_z}, \qquad (1)$$

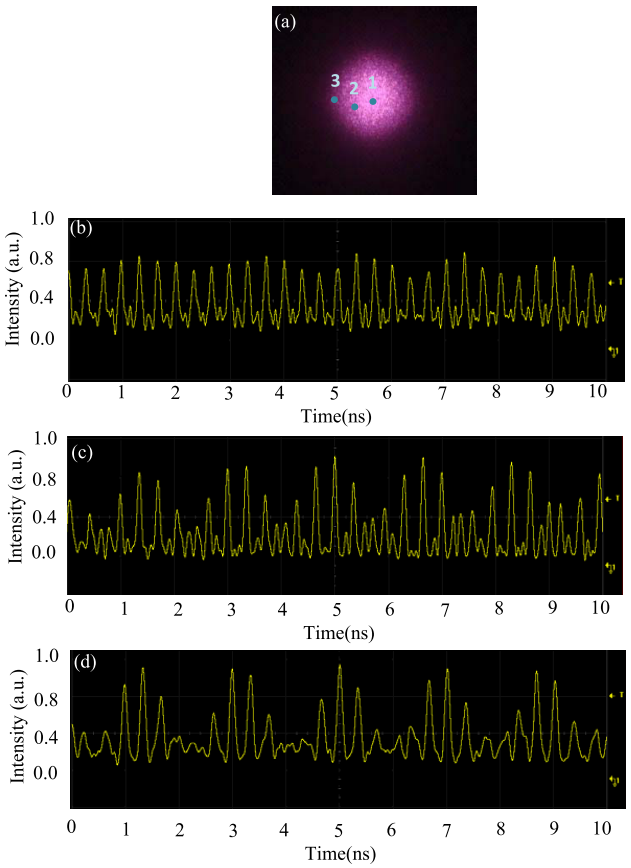

Figure 4. Typical results at an incident pump power of 15.5 W. (a) Experimental mode pattern at a distance of 400 mm from the output coupler; (b)–(d) pulse trains for three positions labeled 1–3 in (a), respectively.

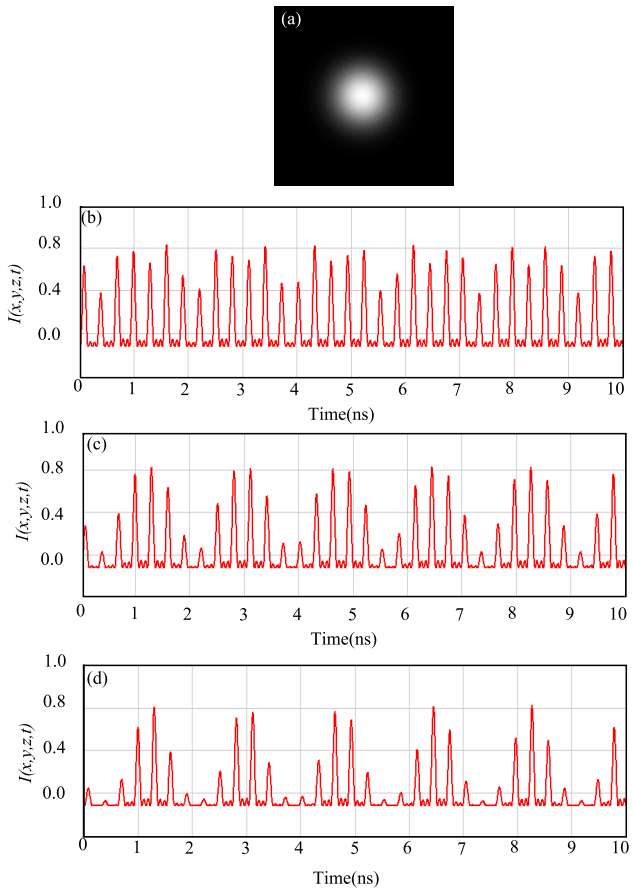

Figure 5. (a)–(d) Numerical results corresponding to experimental observations in figures 4(a)–(d), respectively.

with

$$\psi_{n,m}^{(\mathrm{HG})}(x, y, z, t) = \frac{\sqrt{2}}{\omega(z)}\psi_n(\tilde{x}, \phi)\psi_m(\tilde{y}, \phi), \tag{2}$$

and

$$\psi_n(\xi, \vartheta) = (2^n n!\sqrt{\pi})^{-1/2}\mathrm{e}^{-\xi^2/2}H_n(\xi)\mathrm{e}^{-\mathrm{i}(n+1/2)\,\vartheta}, \tag{3}$$

where $t_z = t-(z/c)[1+(x^2+y^2)/2(z^2+z_R{}^2)]$, $\tilde{\xi} = \sqrt{2}\xi/\omega(z)$, $\omega(z) = \omega_0\sqrt{1+(z/z_R)^2}$, $z_R = \pi\omega_0^2/\lambda$, $\phi = \Omega_\mathrm{T}t_z + \theta(z)$, $\theta(z) = \tan^{-1}(z/z_R)$, where ω_0 is the waist spot size at the cavity flat mirror $z = 0$, λ is the wavelength of the Raman output, Ω_L and Ω_T are the longitudinal and transverse mode spacings, (n, m) are the transverse indices, and l is the longitudinal index. As shown in figure 3(b), the longitudinal and transverse frequency spacings $(\Omega_\mathrm{L}/2\pi, \Omega_\mathrm{T}/2\pi)$ are 2.93 and 0.60 GHz, respectively.

With thorough numerical fitting, we found that the spatiotemporal behavior shown in figures 4(b)–(d) can be reconstructed with the wavefunction

$$E(x, y, z, t) = \sum_{s=0}^{2} a_s[\Psi_{s,0,N}(x, y, z, t) + \Psi_{0,s,N}(x, y, z, t)], \tag{4}$$

with

$$\Psi_{n,m,N}(x, y, z, t) = \frac{1}{\sqrt{N}}\sum_{l=l_0}^{l_0+N}\Phi_{n,m,l}(x, y, z, t). \tag{5}$$

The normalized electric field in equation (5) means the single-transverse-mode (n, m) with $N + 1$ longitudinal modes from the lowest index l_0 with equal amplitudes and phase-locking. The weighting a_s in equation (4) indicates the relative amplitudes of the transverse modes with different orders. We find that the best fittings of a_s for figures 4(b)–(d) are $(a_0, a_1, a_2) = (0.7, 0.5, 0.1)$. Figures 5(b)–(d) present the numerically reconstructed pulse trains corresponding to the experimental results in figures 4(b)–(d), respectively. The corresponding mode pattern was reconstructed as depicted in figure 5(a). The numerical results can be found to be in good agreement with the experimental observations. The excellent agreement confirms that the origin of spatiotemporal dynamics comes from the total mode-locking of fundamental and high-order transverse modes.

4. Conclusions

In conclusion, we have explored the temporal dynamics of diode-pumped Nd:YVO_4 CW self-Raman lasers. We obtained an average output power of 80 mW at the first

Stokes wavelength in the single-transverse-mode operation and found the self-Raman laser to display the characteristics of self-mode-locking. In the multi-transverse-mode operation, the average output power could be up to 1.1 W and the real-time traces exhibited the phenomenon of spatiotemporal dynamics. We have numerically confirmed that the complex spatiotemporal dynamics arise from the total mode-locking of fundamental and high-order transverse modes. Our explorations imply the great potential of such a laser system to be utilized to generate ultrafast light pulses with new wavelengths through the SRS technology.

Acknowledgments

The authors acknowledge the National Science Council of Taiwan for their financial support of this research under contract NSC-100-2628-M-009-001-MY3.

References

[1] Lagatsky A A, Abdolvand A and Kuleshov N V 2000 *Opt. Lett.* **25** 616
[2] Chen W, Inagawa Y, Omatsu T, Tateda M, Takeuchi N and Usuki Y 2001 *Opt. Commun.* **194** 401
[3] Findeisen J, Eichler H J and Peuser P 2000 *Opt. Commun.* **181** 129
[4] Chen Y F 2004 *Opt. Lett.* **29** 2279
[5] Chen Y F 2004 *Opt. Lett.* **29** 2632
[6] Chen Y F 2004 *Opt. Lett.* **29** 1915
[7] Kaminskii A A *et al* 2001 *Opt. Commun.* **194** 201
[8] Cerny P, Jelinkova H, Zverev P G and Basiev T T 2004 Solid state lasers with Raman frequency conversion *Prog. Quantum Electron.* **28** 113–43
[9] Cong Z, Zhang X, Wang Q, Liu Z, Chen X, Fan S, Zhang X, Zhang H, Tao X and Li S 2010 Theoretical and experimental study on the Nd:YAG/$BaWO_4$/KTP yellow laser generating 8.3 W output power *Opt. Express* **18** 12111–8
[10] Chang Y T, Chang H L, Su K W and Chen Y F 2009 High-efficiency *Q*-switched dual-wavelength emission at 1176 and 559 nm with intracavity Raman and sum-frequency generation *Opt. Express* **17** 11892–7
[11] Demidovich A A, Grabtchikov A S, Lisinetskii V A, Burakevich V N, Orlovich V A and Kiefer W 2005 *Opt. Lett.* **30** 1701
[12] Pask H M 2005 *Opt. Lett.* **30** 2454
[13] Savitski V, Friel I, Hastie J, Dawson M, Burns D and Kemp A 2012 *IEEE J. Quantum Electron.* **48** 328
[14] Fan L, Fan Y, Li Y, Zhang H, Wang Q, Wang J and Wang H 2009 *Opt. Lett.* **34** 1687
[15] Lisinetskii V A, Grabtchikov A S, Demidovich A A, Burakevich V N, Orlovich V A and Titov A N 2007 *Appl. Phys.* B **88** 499
[16] Zhu H Y, Duan Y M, Zhang G, Huang C H, Wei Y, Chen W D, Huang L X and Huang Y D 2011 *Appl. Phys.* B **103** 559
[17] Lin J and Pask H M 2012 *Appl. Phys.* B **108** 17
[18] Omatsu T, Okida M, Lee A and Pask H M 2012 *Appl. Phys.* B **108** 73
[19] Statz H and Bass M 1969 *J. Appl. Phys.* **40** 377
[20] Glas P, Naumann M, Schirrmacher A, Däweritz L and Hey R 1999 *Opt. Commun.* **161** 345
[21] Liu H, Nees J and Mourou G 2001 *Opt. Lett.* **26** 1723
[22] Liang H C, Huang Y J, Huang W C, Su K W and Chen Y F 2010 *Opt. Lett.* **35** 4
[23] Liang H C, Chang H L, Huang W C, Su K W, Chen Y F and Chen Y T 2009 *Appl. Phys.* B **97** 451
[24] Lisinetskii V A, Busko D N, Chulkov R V, Grabtchikov A S, Apanasevich P A and Orlovich V A 2005 *Conf. on Lasers and Elecro-Optics Europe (June)*
[25] Chang Y T, Huang Y P, Su K W and Chen Y F 2008 *Opt. Express* **16** 21155
[26] Siegman A E 1986 *Lasers* (Mill Valley, CA: University Science Books)
[27] Auston D H 1968 *IEEE J. Quantum Electron.* **4** 420
[28] Côté D and van Driel H M 1998 *Opt. Lett.* **23** 715
[29] Liang H C, Lee Y C, Tung J C, Su K W, Huang K F and Chen Y F 2012 *Opt. Lett.* **37** 4609